Engineering Structures 240 (2021) 112411

Contents lists available at ScienceDirect

Engineering Structures

journal homepage: www.elsevier.com/locate/engstruct

Testing robustness: A full-scale experimental test on a two-storey reinforced concrete frame with solid slabs

Alejandro Pérez Caldentey [a,b,*], Yolanda G. Diego [a], Freddy Ariñez Fernández [b], Anastasio P. Santos [a]

[a] Universidad Politécnica de Madrid (UPM), Spain
[b] FHECOR Consulting Engineers, Spain

ARTICLE INFO

Keywords:
Robustness
Column removal
Finite element modelling
Damage
Dynamic impact
Factor

ABSTRACT

This paper presents the results of a full-scale robustness test carried out on a two storey building with two square reinforced concrete slabs (25 cm deep) with a span of 6.6 m, in which a corner column was suddenly removed. Despite the extreme action, and the fact that the slab was not designed for it, only relatively minor damage was observed, with a maximum deflection around 22 cm and apparently controled cracking patterns. The slab started working as a simply supported element along the symmetry axis of the structure supported on only 3 columns. The tests was modeled using Finite Element Analysis. It was observed that the model could capture very well the behaviour of the real structure, predicting very similar cracking patterns and deflections. The structure was shored two hours after the test because deflections were not yet fully stabilized. It is suspected that this increase of deflections could be related to the deterioration by torsional effects of the connection between the slab and columns on the first floor.

1. Introduction

The modern concept of *Robustness* as currently understood in the field of structural engineering is a concept that was coined after the Ronan Point failure in 1968 [23] where a relatively small gas explosion in a buiding designed with prefabricated elements resulted in the failure of the whole corner of the building. Eurocode 1 in Part 1.7 [10] defines the concept of *Robustness* as follows:

"the ability of a structure to withstand events like fire, explosions, impact, or the consequences of human error, without being damaged to an extent disproportionate to the original cause."

Design for robustnes is dealt with in several design standards and guides. ASCE/SEI [2] establishes two direct strategies (Alternative Path Method and Specific Local Resistance Method) and one indirect strategy (Indirect Method) to avoid progressive collapse. GSA [14] develops the Alternate Path Method and includes specific requirements for reinforced concrete, structural steel, wood, masonry and cold-formed steel structures. NIST [24] provides further guidance on how to apply both direct and indirect methods as defined in ASCE/SEI-7-16. Finally, DoD [11] classifies structures according to their Risk Category and establishes minimum requirements for each category, going from tie requirements to the alternate path method to Enhanced Local Resistance for the most stringent structure category class. This publication also deals with different materials and establishes conditions for connections as well as acceptance criteria.

These methods are developed and applied to specific cases in several other publications. Among them Krauthammer [17], fosuses on the importance of connections both in steel and concrete structures. Kunnath et al. [18] provide an overview of design methods and experimental results focused mainly on the Alternate Path Method. Marjanishvili [20] elaborates on different analysis procedures to assess the risk of progressive collapse going from the simplest (linear-elastic static analysis) to the most complex (nonlinear dynamic analysis). Bao et al. [4] use macromodel techniques where joints are represented by a series of non-linear springs to simulate the behaviour of building structures subjected to sudden column removal. They successfully compare their results to refined FEM calculations for buildings designed accounting and not accounting for seismic actions. Lee et al. [19] present a simplified analysis of column removal in 2D steel frames based on assuming a trilinear Force-Rotation diagram and using energy-based principles. Brunesi et al. [5] analyse examples of 2D and 3D RC frame structures, under different column removal scenarios, using a fibre-based software implemented into Opensees and SeismoStruct and validate the calculations using LS-Dyna. Comparison to current code provisions reveal that code provisions are over-conservative. Eren et al.

* Corresponding author.

https://doi.org/10.1016/j.engstruct.2021.112411
Received 23 July 2020; Received in revised form 24 March 2021; Accepted 14 April 2021
Available online 4 May 2021

Notation

Following is a definition of all the symbols used in the paragraphs above.

A_s	area of required tensile flexural reinforcement per meter of slab
$A_{s,sup}/w$	area of reinforcement actually placed on the top face of the slab in the vicinity of the columns per meter of slab
A_{sw}	punching reinforcement in one perimeter surrounding the support
G_1	self-weight
G_2	supwerimposed dead load
L	span (6.6 m)
M_0	isostatic bending moment corresponding to the full width of the slab
$M^+_{Ed,central}$	Positive design bending moment corresponding to the central strip
$M^+_{Ed,column}$	Positive design bending moment corresponding to the column strip
Q	live load
I_{cr}	moment of inertia of the cracked cross section
I_g	moment of inertia of the gross cross section
d	effective height of the slabs (0.20 m)
f_{yd}	factored yield stress of reinforcement
$f_{ywd,ef}$	effective stress in the reinforcemnet, accounting for the fact that for small heights of slab the shear reinforcement does not achieve full yielding
s_r	distance between punching reinforcement perimeters
q_{Ed}	uniform factored load per square meter
u_1	perimeter of the control section used for punching verification
v_{Ed}	factored punching stress at the control perimeter
v_{Rd}	factored punching stress at the control perimeter that can be resisted by concrete without shear reinforcement
w	width of the slab (7.0 m)
w_c	width of the column or central strip (3.5 m)
x_{cr}	depth of the cracked neutral axis
α_e	modular ratio $= E_c/E_s$
β	factor accounting for the eccentricity between the axial force in the support and the control perimeter, as well as for unbalanced moments
γ_c	Partial factor applied on the resistance of concrete (1.5)

[12] investigate the influence of masonry infills on the resistance of RC frame buildings to collapse by sudden column removal. The paper uses a macro-model approach, validated by comparison to 1/3 scale tests of a planar structure, to simulate several scenarios and concludes that masonry infills can significantly increase the resistance of structures to column removal.

There are attempts to establish more general design procedures based on the concept of fragility for concrete frame structures, based on incremental dynamic analysis [7], and push down analysis [6]. Parisi et al. [25] also attempt to establish *perfomance limit states* for RC concrete frames.

Regarding experimental studies, Alshaikh et al. [1] provide an interesting overview of experimental results focusing on the effects of important variables such as type of structure, boundary conditions, detailing, masonry infills and so on.

Some experimental studies carried out to study the robustness of structures in reduced scale models include [3,29,30,31,28,36,35,38], the first ones motivated by the Ronan Point collapse.

There are also a few examples which correspond to tests of real buildings before demolition. For instance, Sasani [32] removed two columns from a reinforced concrete frame structure before demolition. The columns were removed using explosives so that dynamic effects were fully accounted for. Also, Song et al. [33] removed four columns (two interior columns and two columns adjacent to a corner) from a steel structure before demolition. The removal, however was made by cutting the columns by torching and was not fully dynamic. Such tests are of great value but are also affected by the complex geometries of the buildings and their analysis has to deal with the uncertianties pertaining to the material properties, as is always the case when dealing with the assessment of existing structures.

There are very few tests involving full-scale models tested in controlled laboratory conditions.Adam [16] tested a full-scale reinforced concrete building consisting of two spans each way with a span length of 5.00 m and with two floors subjected to the removal of a corner column. Another full-scale test of the reproduction of a part of a building (one storey only, with 6 columns) with composite formed steel deck is presented by Wang et al. [34]. In this case the spans were rather small 3.6x4.2 m and the tests was carried out by applying load statically at the location of an edge column. Finally, Zandonini et al. [37] tested a 2x2 span with a span length of 5.7 m corresponding a one-storey steel frame with a composite steel–concrete floor. The test was carried out in three phases: column removal, stabilization and push down test until failure was reached. Failure was at the beam to column bolted connection.

So even though some full scale tests are available, they correspond to very particular scenarios and are very far from covering the different structural typologies of real structures. For this reason, test that can fill some of the gaps in the pool of experimental results are quite valuable and necessary for the validation of numerical models.

This paper describes the results of one such test dealing with a full scale robustness test consisting in suddenly removing a column from a two-storey building built inside the Structures' Laboratory of the Universidad Politécnica de Madrid (UPM). The structure consists of two reinforced concrete slabs having an area of seven by seven meters each supported on 4 columns, with a span between columns equal to 6.6 m. One of the columns is suddenly removed. This is achieved by manufacturing this column in steel and providing it with 3 hinges. The central hinge was blocked during construction and released for the test. The rest of the columns are reinforced concrete columns.

The structure was designed as a normal reinforced concrete building without providing any special measures to account for the accidental action to which it was submitted.

The test has been modelled using LS-DYNA Finite Elements code [15] obtaining results that closely mirror the experimental ones, both in terms of displacements as well as in terms of the observed cracking patterns.

2. Test description

2.1. Structure geometry

The structure consists of two 25 cm slabs with external dimensions of 7x7 m^2, supported on 4 columns with spans of 6.60 m. As can be seen in

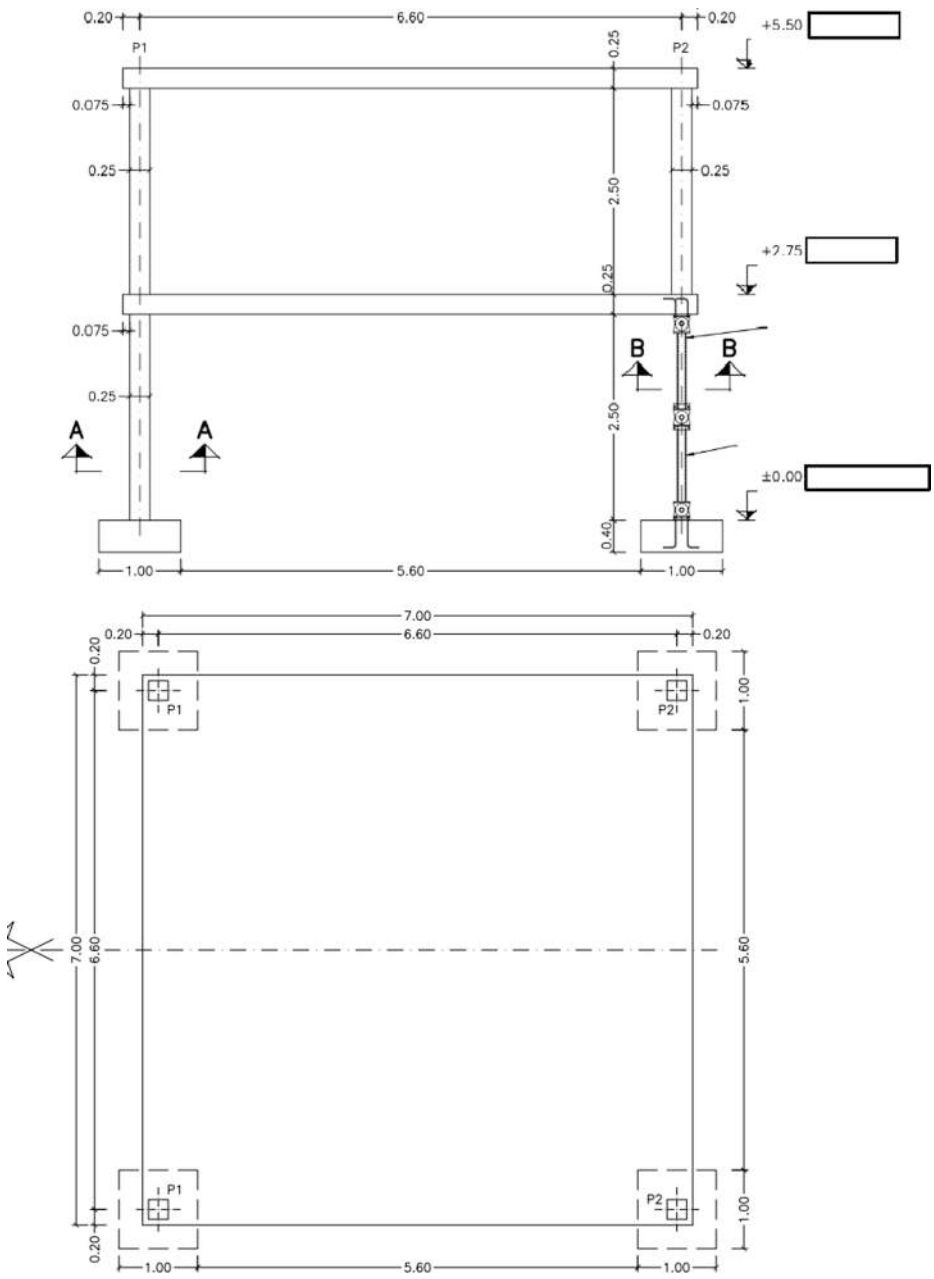

Fig. 1. Structure elevation and plan view.

Fig. 1, the supports are 25x25 cm^2 reinforced concrete elements, with the exception of one of those going from the foundation to the first storey. This support is made by two welded UPE-100 profiles and is equiped with 3 hinges and a mechanism to block the central hinge, to guarantee stability during construction.

The flexural reinforcement of the slabs is shown in Fig. 2. It consists in a 16 mm bar mesh spaced at 20 cm placed on the bottom of face and a 12 mm bar mesh spaced at 20 cm placed on the top face. Additionally a supplementary reinforcement for positive bending consisting in 12 mm bars spaced at 20 cm is placed on the bottom face in the column strip (1/4 of the transversal span in the vicinity of the columns). Additionally, punching reinforcement is provided as shown in Fig. 3. Punching reinforcement consists in a total of eighteen 12 mm links. The detail used is unconventional from a theoretical point of view, since the links do not embrace the main flexural reinforcement (instead they are held together by auxiliary 8 mm bars), but this is a detail commonly used in construction and there is experimental evidence that it functions properly [26]. It was decided to use this detail to account for actual construction practices.

The reinforcement of the supports consists in 4, 12 mm bars on the corners with 12 mm stirrups spaced at 10 mm in the top and bottom 50 cm and spaced at 20 cm in the central part of the supports. The stirrups are also placed at 10 cm as the column goes through the slab.

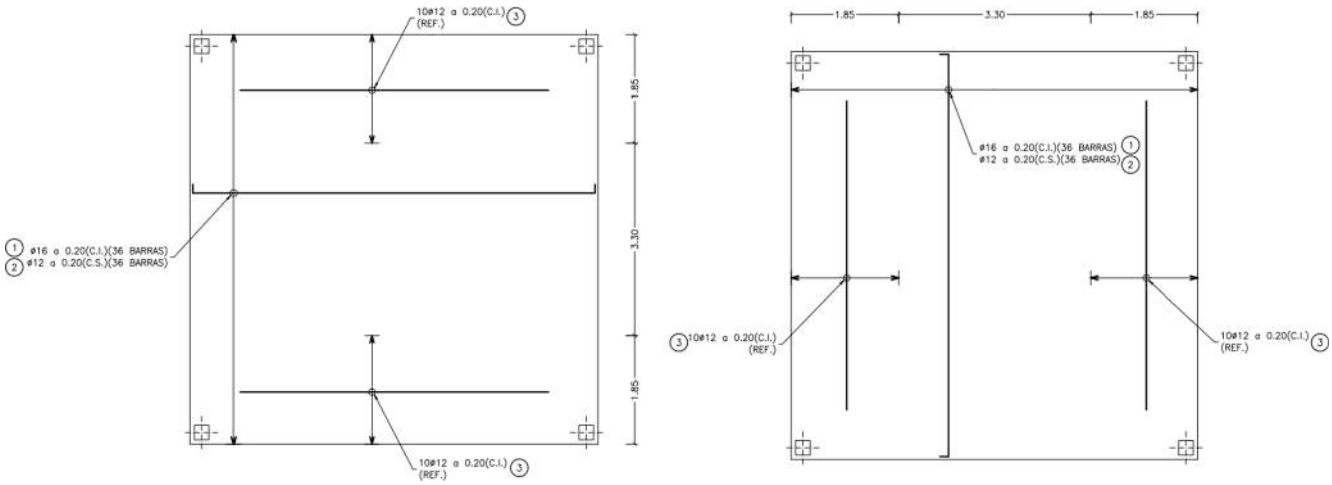

Fig. 2. Slab reinforcement.

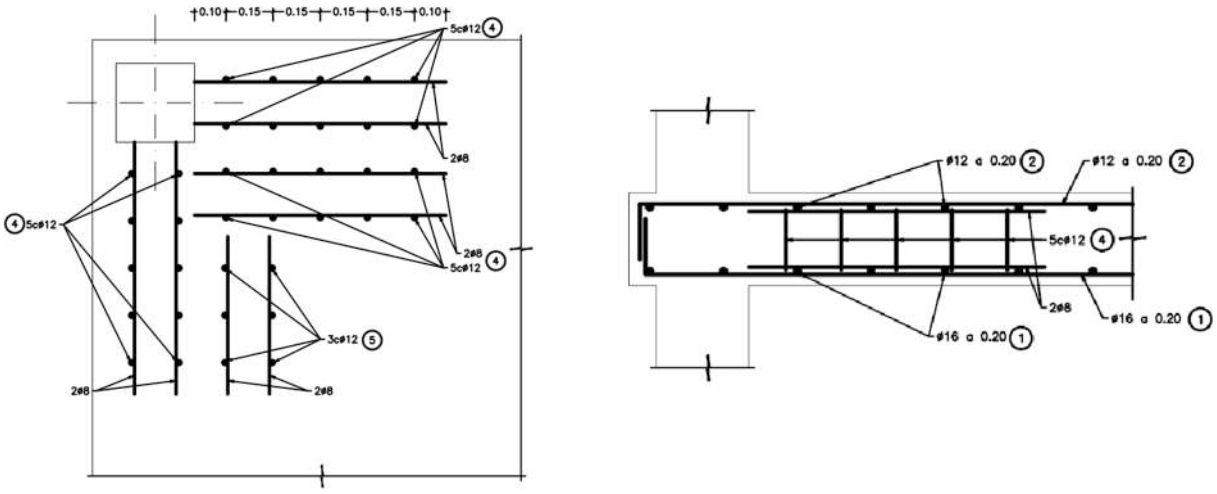

Fig. 3. Punching reinforcement (left: plan view; right elevation).

Fig. 4. View of the structure built inside the laboratory.

2.2. Design of reinforcement

The reinforcement of the slab was determined assuming the following loads:

- Self-weight: $G_1 = 0.25 \times 25 = 6.25$ kN/m^2
- Superimposed dead load: $G_2 = 1.5$ kN/m^2
- Live load: $Q = 4.0$ kN/m^2

The direct dimensioning method for slabs as described in [13] is used to determine the bending moments and their distribution between the column strip and the central strip. Eq. (1) details the dimensioning of the flexural slab reinforcement. Due to the uncertainties in the value of the superimposed dead load G_2, a partial factor of 1.5 is applied to this load. A B 500C steel has been assumed. All symbols are at the begining of the paper.

$$M_0 = q_{Ed}\frac{L^2}{8} = (\gamma_{G_1}G_1 + \gamma_{G_2}G_2 + \gamma_Q Q)w\frac{L^2}{8} = (1.35 \times 6.25 + 1.5 \times (1.5 + 4)) \times 7 \times \frac{6.6^2}{8} = 636.04\ kNm$$

$$M^+_{Ed,column} = 0.6M_0 = 0.6 \times 636.04 = 381.63\ kNm\rightarrow$$

$$A_s \approx \frac{0.6M_0}{0.9 \times d}\frac{1}{f_{yd}}\frac{2}{w_c} = \frac{381.63}{0.9 \times 0.2}\frac{1.15}{50}\frac{1}{3.5} = 13.93\ cm^2/m \rightarrow (\phi 16 + \phi 12)@0.2 = 15.7\ cm^2/m \quad (1)$$

$$M^+_{Ed,central} = 0.4M_0 = 254.42\ kNm\rightarrow$$

$$A_s \approx \frac{0.4M_0}{0.9 \times d}\frac{1}{f_{yd}}\frac{2}{w_c} = \frac{254.42}{0.9 \times 0.2}\frac{1.15}{50}\frac{1}{3.5} = 9.29\ cm^2/m \rightarrow \phi 16@0.2 = 10.05\ cm^2/m$$

For the dimensioning of the punching reinforcement, EN 1992-1-1:2004 [9] has been used, as detailed in Eq. (2).

$$v_{Ed} = \beta q_{Ed}\frac{w^2}{4u_1} = 1.5\underbrace{(1.35 \times 6.25 + 1.5 \times (1.5 + 4))}_{16.69} \times \frac{7^2}{\underbrace{4\left(0.25 \times 2 + \frac{\pi}{2}2 \times 0.2\right)}_{1.13}}\frac{1}{0.20} = 1.35\ MPa$$

$$v_{Rdc} = \frac{0.18}{\gamma_c}\left(1 + \sqrt{\frac{200}{d[mm]}}\right)\left(100\frac{A_{s,sup}/w}{100 \times d}25\right)^{\frac{1}{3}} = \frac{0.18}{1.5}\left(1 + \sqrt{\frac{200}{200}}\right)\left(100\frac{5.65}{100 \times 20}25\right)^{\frac{1}{3}} = \quad (2)$$

$$= 0.46\ MPa$$

$$\frac{A_{sw}}{s_r} = \frac{(v_{Ed} - 0.75 \times v_{Rdc})}{1.5d\ \underbrace{f_{ywd,ef}}_{250+0.25d[mm]\ in\ MPa}\ sin\alpha}u_1 d = \frac{(1.35 - 0.75 \times 0.46) \times 1000}{1.5 \times 0.2 \times \frac{(250 + 0.25 \times 200)}{10}}1.13 \times 0.2 = 25.91\ cm^2/m$$

Fig. 4 shows the structure built inside the lab. The dotted pattern on the side of the lower slab was used to measure the time-history of deflections along the edge of the slab during the test using Digital Image Correlation (DIC).

Fig. 5 shows the detail and materialization of the central hinge of the steel column. The hinge is blocked by inserting 4 horizontal 20 mm steel rods though the 21 mm holes in the top and bottom vertical plates.

3. Test description

3.1. Test description

The test was carried out on May 4th, 2016. To carry out the test a hydraulic jack (yellow jack in Fig. 5) was placed in series with a manual jack (green jack in Fig. 5) at the point of the central hinge on the steel support. The manual jack was used to achieve good contact and a minimum level of pressure between the jack and the support. The steel support was designed so that it would be built with a slight rotation at the central hinge, so that the jack would serve as a support for the structure once the central hinge was liberated.

The four horizontal rods used to block the central hinge had a circular plates welded to them at one of the ends. It was then possible to attach a cable around the circular plate and pull the rods out using a jack placed perpendicularly to the supporting jacks. Once this operation was carried out successfully, the hydraulic jack pushed the support at the hinge, straightened the support and eventually originated its instability producing a sudden absence of support at the corner of the structure. The structure went down, at that point by approximately 22 cm.

3.2. Monitoring

The monitoring of the structure consisted in the following:

– 2D Digital image correlation (DIC) was used to follow the displacement, velocities and accelerations of one of the edges of the structure. For this, one of the edges of the structure was painted with a pattern of black circles (see Fig. 4). A high speed camera set for 5000 frames per second and a resolution of 512x512 was used. As the objective was to obtain as large a view as possible of the side of the slab going from the corner in which the column was removed to the adjacent column, to follow the deflections of this surface, the pattern

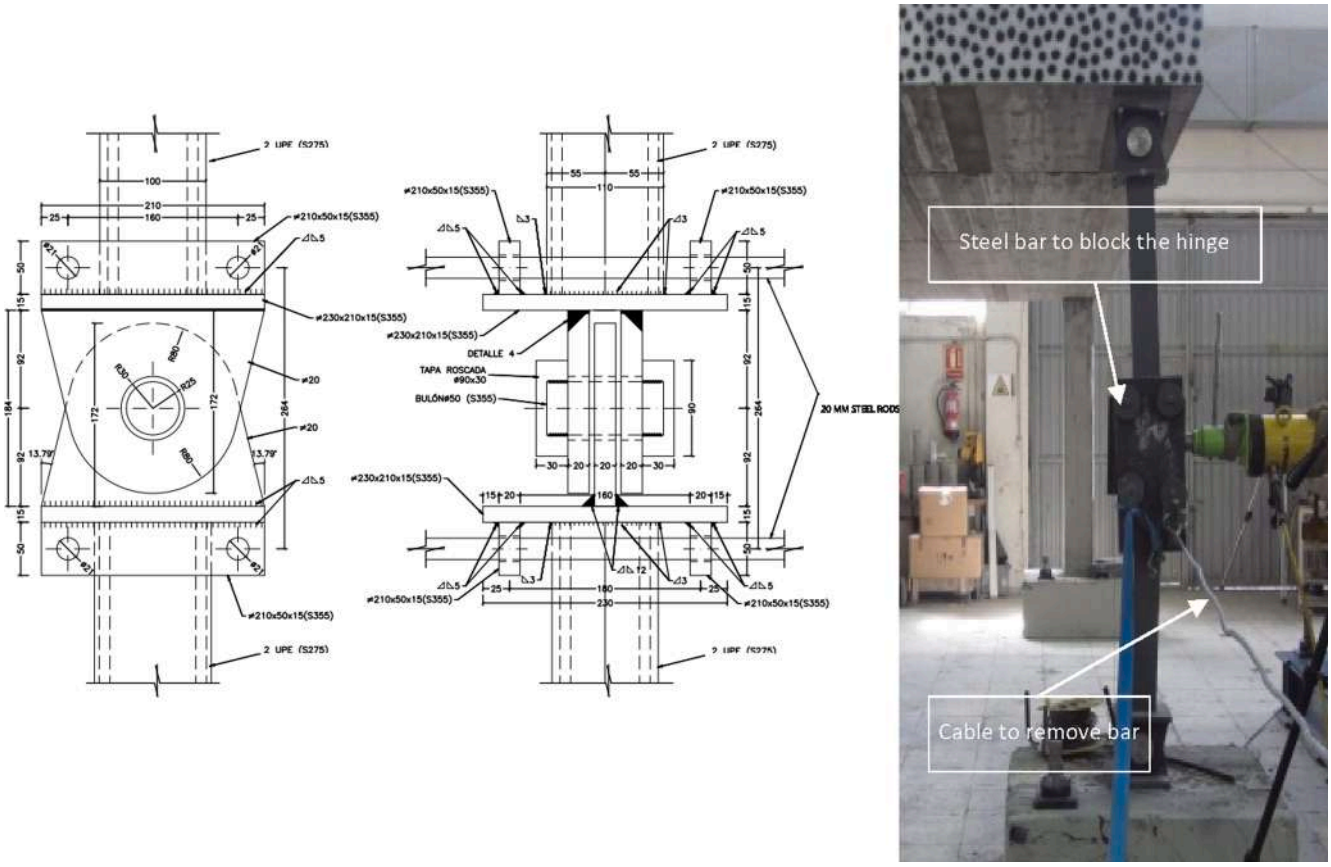

Fig. 5. Detail of central column hinge and view of the built specimen.

was rather coarse and was not meant to measure strains or crack openings.

- Accelerometers were located on the slab corners where the column is removed on both the top and the bottom slab. The acelerometers, had a measuring range of 20 g and were set up with a measurement frequency of 1200 Hz and a Butterworth lowpass filter having a frequency of 250 Hz. The resolution of the accelerometers was 0.0001 g.
- Accelerometers, having the same characteristics, were also located at the centre span of both the top and bottom slab.
- A 3d laser-scan was taken of the full structure before and after the test so that the deflection due to the removal of the column could be determined at any point of the structure. The laser scanner used was Leica Nova MS 60 and was set up with a resolution of 2 cm.
- The compressive strength tests of 150x300 mm concrete cylinder specimens taken from the concrete used to build the columns and slabs was determined for different ages (see Table 3 below). The compressive strength tests were carried out using a compression press with 2000 kN of capacity.

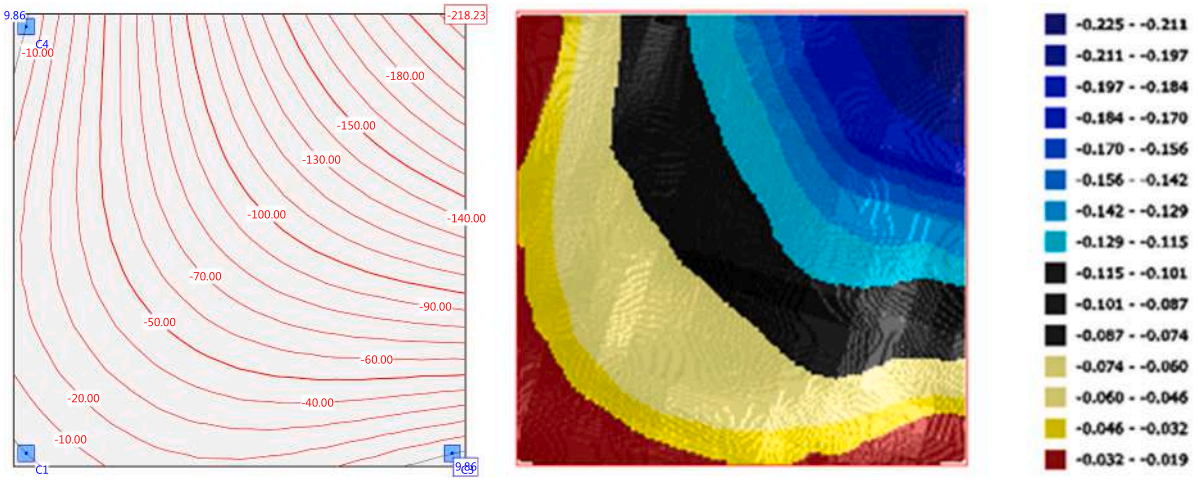

Fig. 6. Left: Deflections assuming a cracked stiffness (in millimeters). Right: Measured deflection in meters.

Table 1
MAT_CSCM_CONCRETE parameters.

Parameter	LS-DYNA symbol	Value
Mass density	RO	2300 Kg/m^3
Unconfined compression strength	FPC	30 MPa
Maximum aggregate size	DAGG	20 mm
Erode parameter	ERODE	1.1

Table 2
Parameters for piecewise linear plasticity material model for steel rebars.

Parameter	LS-DYNA symbol	Value
Mass density	RO	7850 kg/m^3
Young's modulus	E	210 GPa
Poisson's ratio	PR	0.3
Yield stress	SIGY	575 MPa
Tangent modulus	ETAN	422 MPa
Effective plastic strain to failure	FAIL	0.075

4. Analysis

4.1. Simplified linear approximation

A very simple analysis was carried out to obtain a first estimate of the results. This analysis consists in assuming a linear elastic calculation with a stiffness equal to the cracked stiffness of the section. The cracked stiffness is determined according to the reinforcement provided for the column strip as detailed in Eq. (3), where it can be seen that it corresponds to 20% of the gross cross-section stiffness.

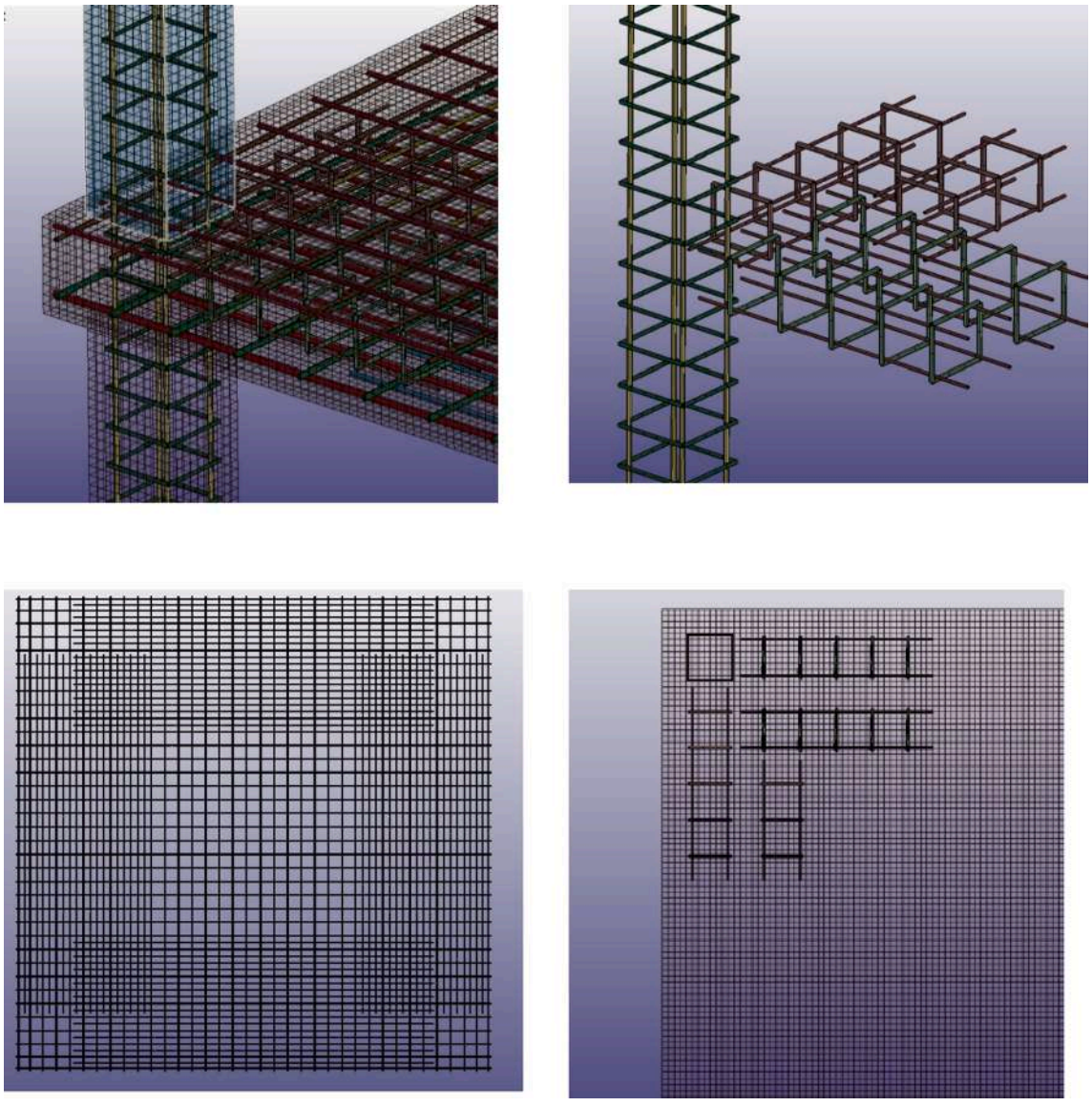

Fig. 7. FEM model details.

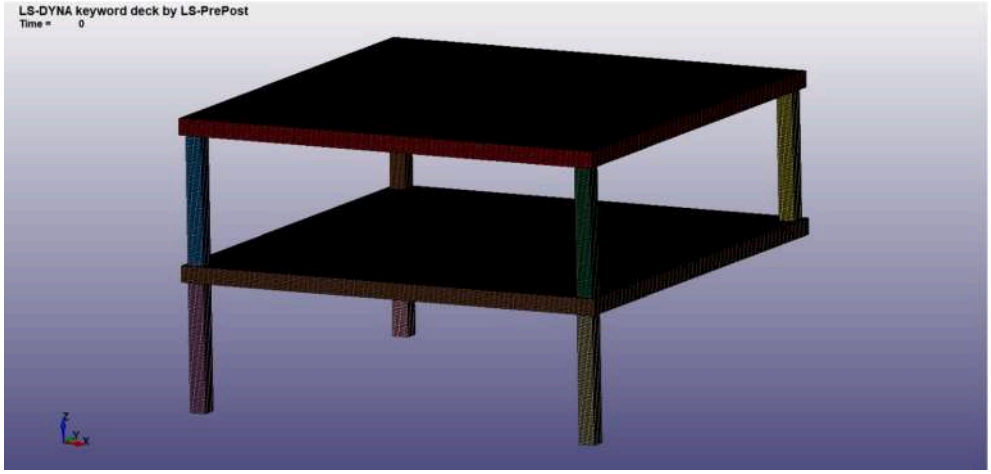

Fig. 8. FEM model.

Table 3
Concrete strength.

Slabs						
Bottom slab				Top slab		
Age [days]	Specimen #	Strength [MPa]	Mean values	Age [days]	Strength [MPa]	Mean values
14	1	30.22	29.27	33	25.28	25.32
	2	29.21		33	27.33	
	3	28.37		33	23.35	
89	1	35.55	35.15	91	29.3	30.72
	2	29.213		91	30.84	
	3	40.6725		91	32.02	
Columns						
Columns supporting the lower slab				Columns supporting the top slab		
21	1	23.38	24.91	36	32.91	30.51
	2	26.36		36	23.85	
	3	25		36	34.76	
93	1	30.17	30.78	91	34.53	35.09
	2	30.76		91	34.68	
	3	31.42		91	36.05	

$$\alpha_e = \frac{E_s}{E_c} = \frac{200}{22\left(\frac{30+8}{10}\right)^{0.3}} = 6.09$$

$$A_s = (\phi 16 + \phi 12)@0.2 = 15.7\ cm^2/m$$

$$x_{cr} = -\alpha_e \frac{A_s}{b} + \sqrt{\left(\alpha_e \frac{A_s}{b}\right)^2 + 2\alpha_e \frac{A_s d}{b}} =$$

$$= -6.09\frac{15.7}{100} + \sqrt{\left(6.09\frac{15.7}{100}\right)^2 + 2 \times 6.09\frac{15.7 \times 20}{100}} = 5.30\ cm$$

$$I_{cr} = \frac{1}{3} b x_{cr}^3 + \alpha_e A_s (d - x_{cr})^2 =$$

$$= \frac{1}{3} 1.00 \times 0.053^3 + 6.09 \times 15.7 \times 10^{-4}(0.2 - 0.053)^2 = 2.562 \times 10^{-4}\ m^4$$

$$\frac{I_{cr}}{I_g} = \frac{2.562 \times 10^{-4}}{\frac{1}{12} 1.00 \times 0.25^3} \approx 0.2 \tag{3}$$

Fig. 6 shows a comparison of this approximation to the actual measured slab deformation. It can be seen that a very good approximation is obtained using this method. Errors that tend to overestimate the deflection (no consideration of Tension stiffening effects) compensate with errors that tend to underestimate the deflection (assumption that all the slab is reinforced uniformly with the reinforcement of the column strip). This approximation could, of course be refined by discriminating the stiffness by zones and by applying a method to account for tension-stiffening, such as the ζ-method [9]. Instead, in the next paragraph a more rigourous analysis using LS-DYNA will be presented. In any case, this very simple analysis shows that the behaviour of the structure is not far from that of cracked behaviour of reinforced concrete, without significant plastic deformations, which, in itself, is surprising given the action. This is also supported by the cracking pattern of the underside of the slabs which is mainly a well-controlled serviceability-type cracking pattern (see paragraph 5).

Table 4
Estimated concrete strength of the different elements at testing.

Element	Age when tested [days]	Estimated concrete strength at time of test [MPa]
Bottom Slab	26	34.55
Top Slab	20	23.71
Columns supporting the bot. Slab	28	26.42
Columns supporting the top Slab	23	28.04

4.2. Finite element model

For the development of the finite element model, the explicit finite element software LS-DYNA [15] is used due to its numerical stability and variety of constitutive models. Eight node solid hexahedron elements are used to simulate concrete parts. The reinforced bars are modeled explicitly using two node Hughes-Liu beam elements with 2x2 Gauss points in the cross section and located in the exact position within the concrete mesh. The interface between reinforcement and concrete is modeled using CONSTRAINED_LAGRANGE_IN_SOLID. Model fixed boundary conditions are applied at the bottom of each column. The maximum size of slab element is 0.025 m for optimal accuracy and computational cost.

In this study, the CSCM model is used to simulate the concrete behaviour. This material model can achieve stable results and several researches have proven its accuracy in the simulation of reinfored concrete subjected to sudden column removal [27]. This model is isotropic and has different response in tension and compression, three plasticity surfaces, softening in compression, damage in tension, and erosion formulation for the elimination of material. This concrete model

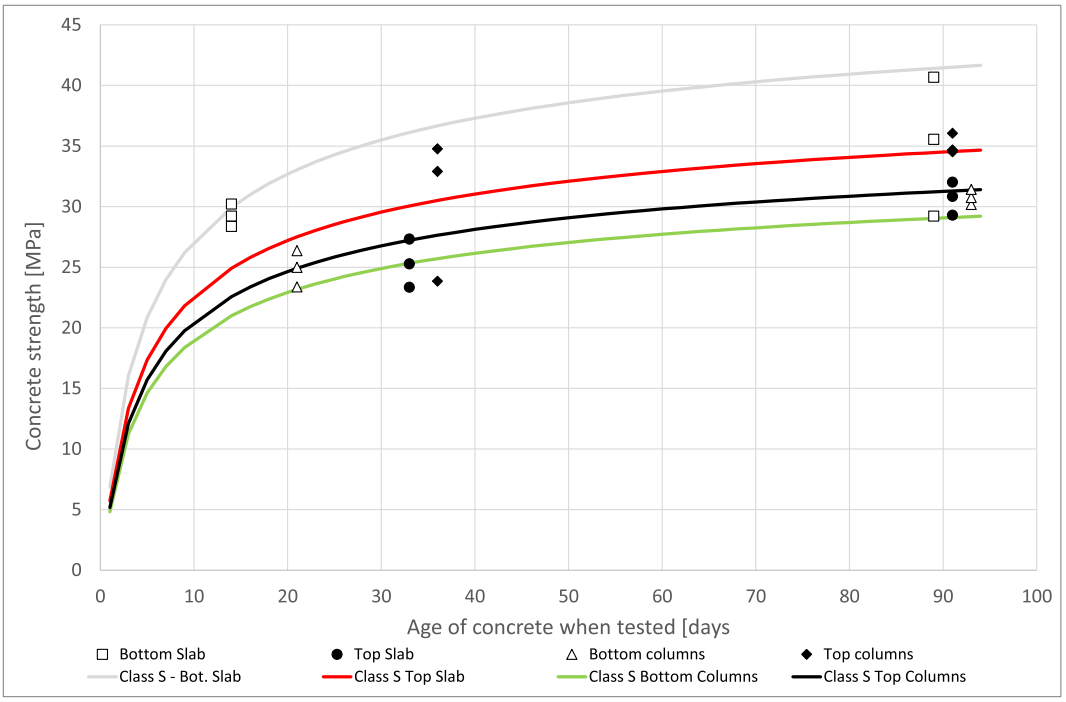

Fig. 9. Measured concrete resistance and estimated evolution in time.

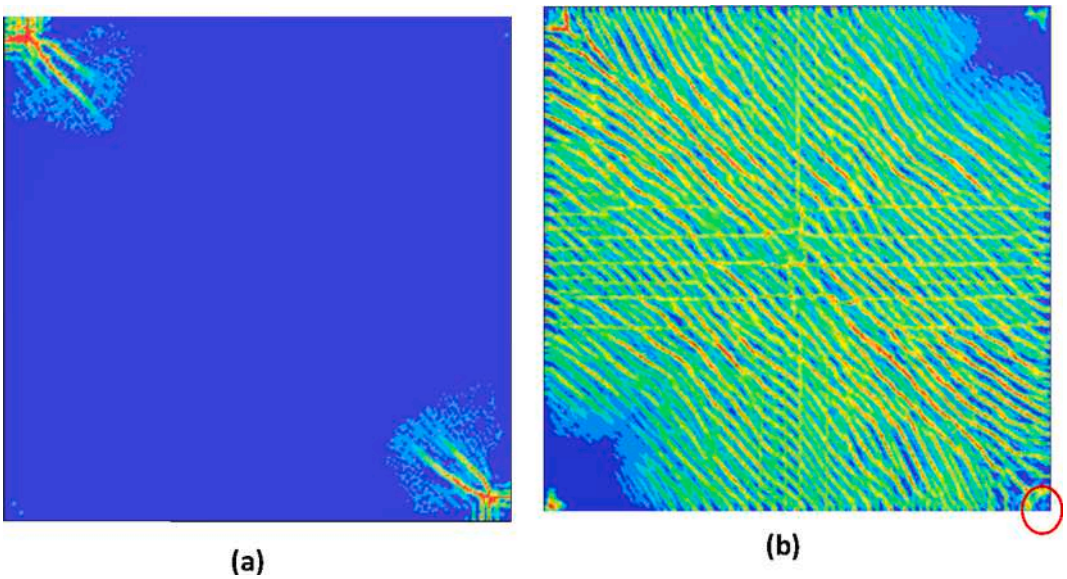

Fig. 10. FEM crack pattern of Top Slab: Top view (a) and (b) Bottom view.

in LS-DYNA is provided based on three input specifications: the uncofined compression strength, the aggregate size, and the units. The uncofined compression strength affects stiffness, strength, hardening, and softening. The CSCM model is valid for normal compressive strengths from 28 MPa to 58 MPa. The aggregate size affects the brittleness of the softening behavior of the damage formulation [22].

Table 1 shows the parameters used for the material model MAT_CSCM_CONCRETE.

The steel behaviour is represented using the Piecewise Linear Plasticity material model, which is an elastoplastic material model with hardening, equal response in tension and compression, and failure when the effective plastic strain reaches the ultimate strain (see Table 2).

LS-DYNA provides different solid element formulations. One integration point at the center of the element is used for modeling concrete in this study. This solid element formulation has three translational degrees of freedom at each node. Although a single point integration formulation is effective for modeling nonlinear material behavior and capturing large deformations, it does suffer from hourglassing or zero-energy modes. To avoid zeroenergy deformations, or hourglassing, an artificial stiffness is added to the eigth node solid elements to resist these zero-energy deformation modes using CONTROL_HOURGLASS in LS-DYNA.

The initial state of the structure under the gravity load is achieved though a dynamic relaxation state. Next, the column is removed, triggering the process.

Fig. 7 shows details of the model where the size of the concrete elements (2.5 cm) as well as the modelling of the reinfocement can be seen. Fig. 8 shows a global view of the LS-DYNA model.

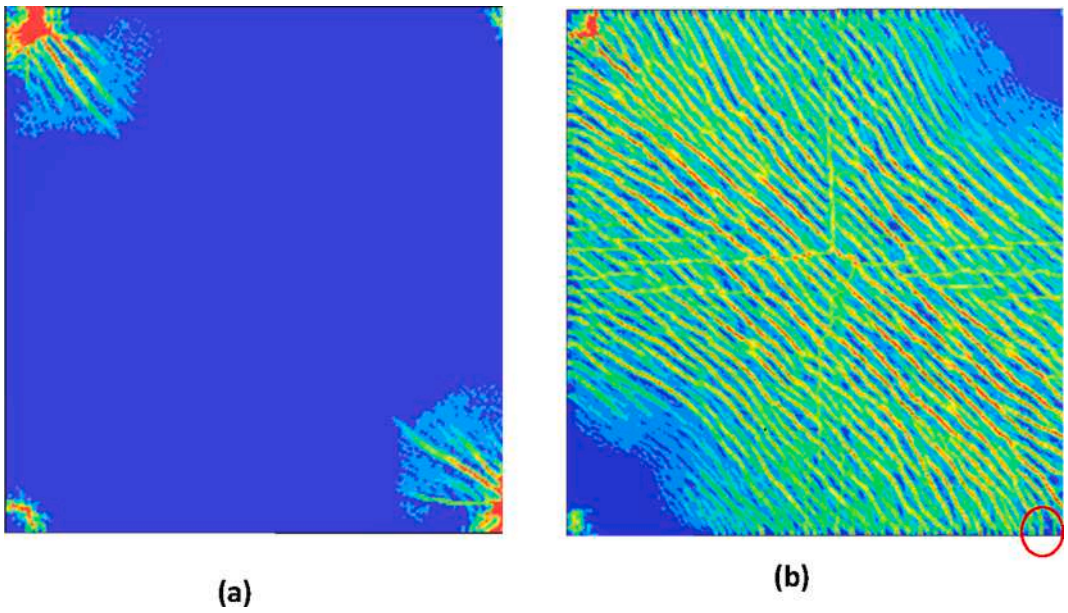

Fig. 11. FEM crack pattern of Bottom Slab: Top view (a) and (b) Bottom view.

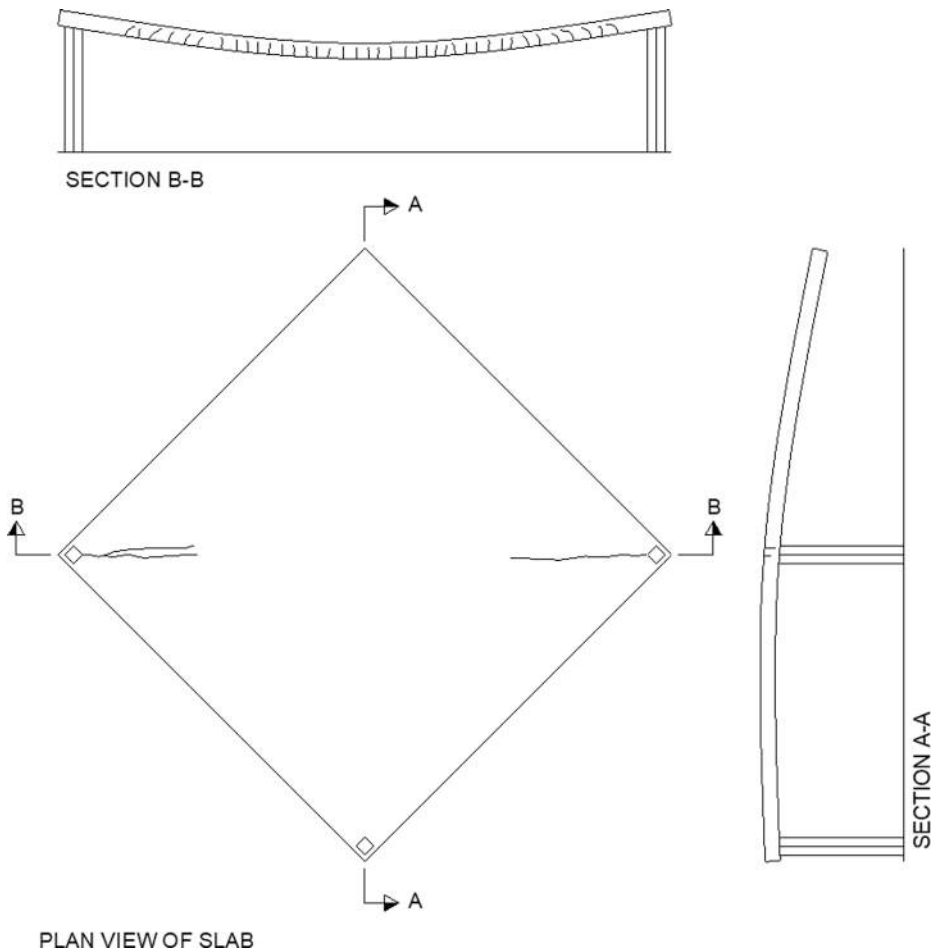

Fig. 12. Deformation and cracking pattern (conceptual scheme). Cantilever behaviour along A-A and simply supported behaviour along section B-B. Vertical deflections exaggerated.

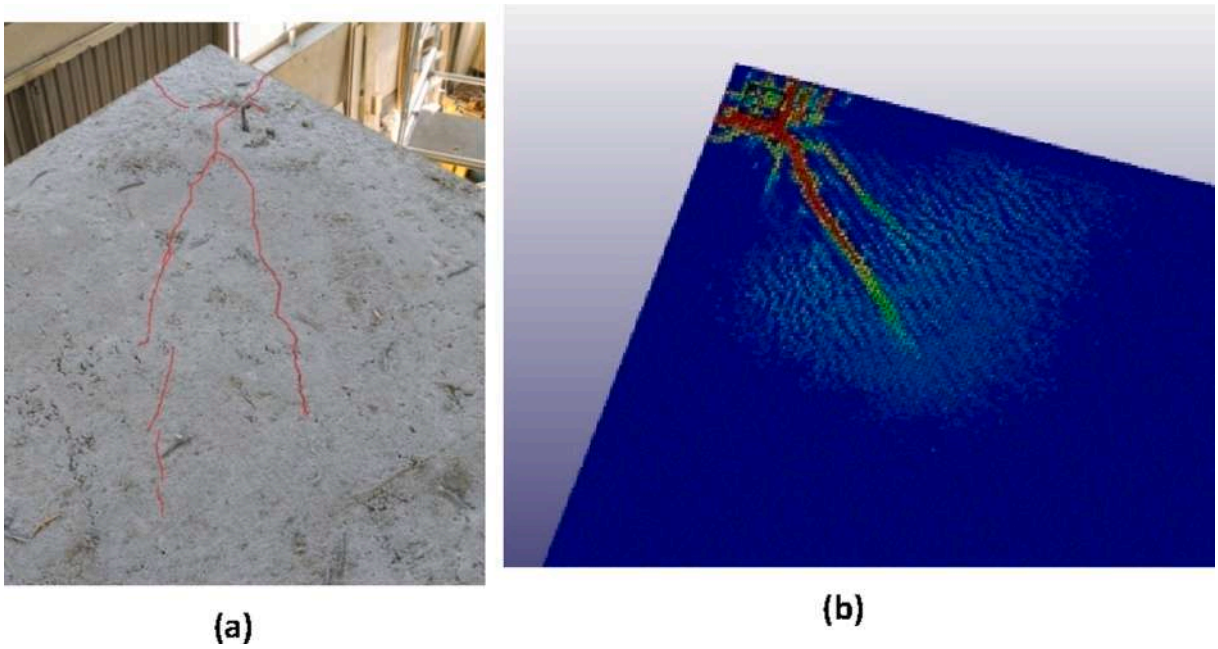

Fig. 13. Test (a) and FEM (b) top corner crack pattern.

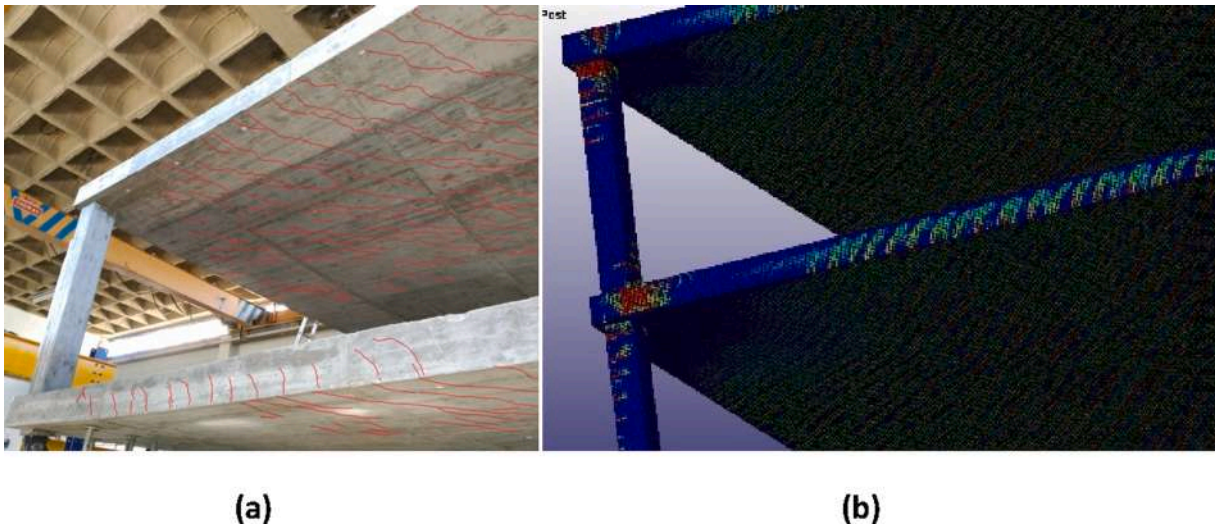

Fig. 14. Test (a) and FEM (b) top slab crack pattern.

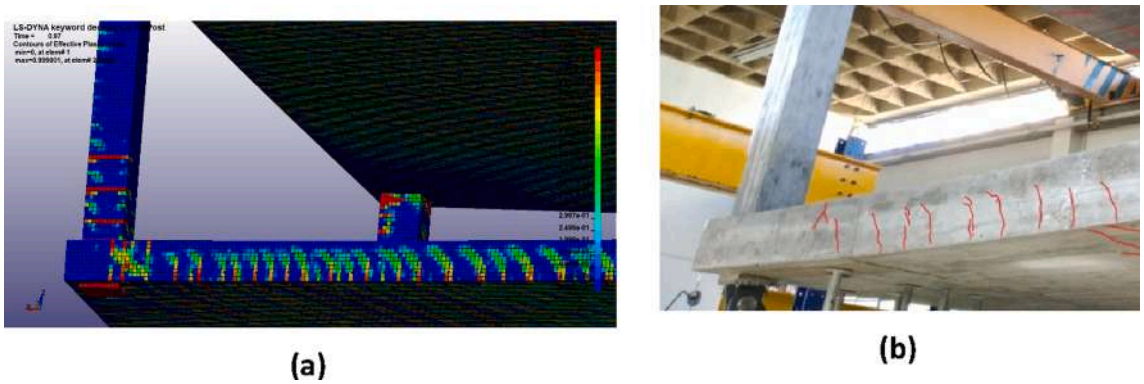

Fig. 15. Test (a) and FEM (b) slab crack pattern.

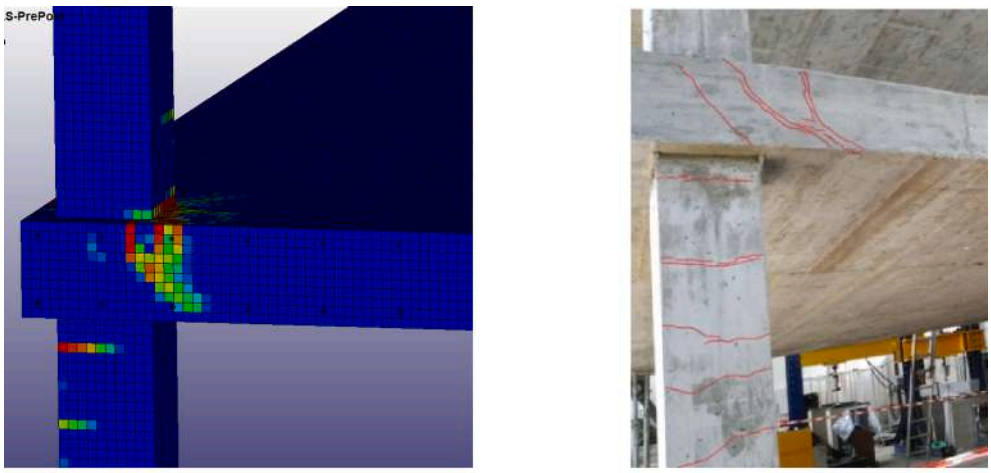

Fig. 16. Test (a) and FEM (b) column- slab crack pattern.

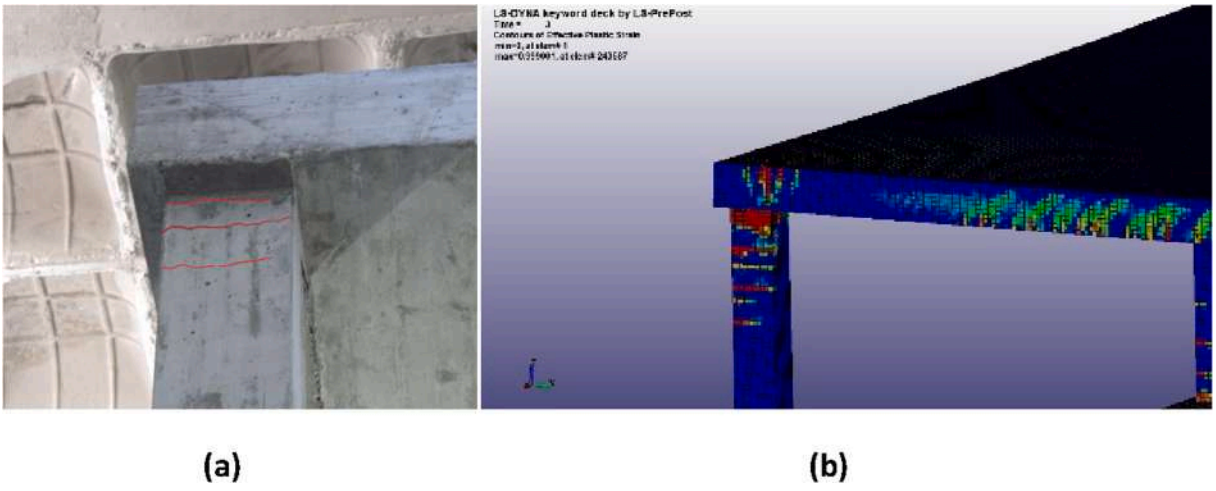

Fig. 17. Test (a) and FEM (b) top slab crack pattern.

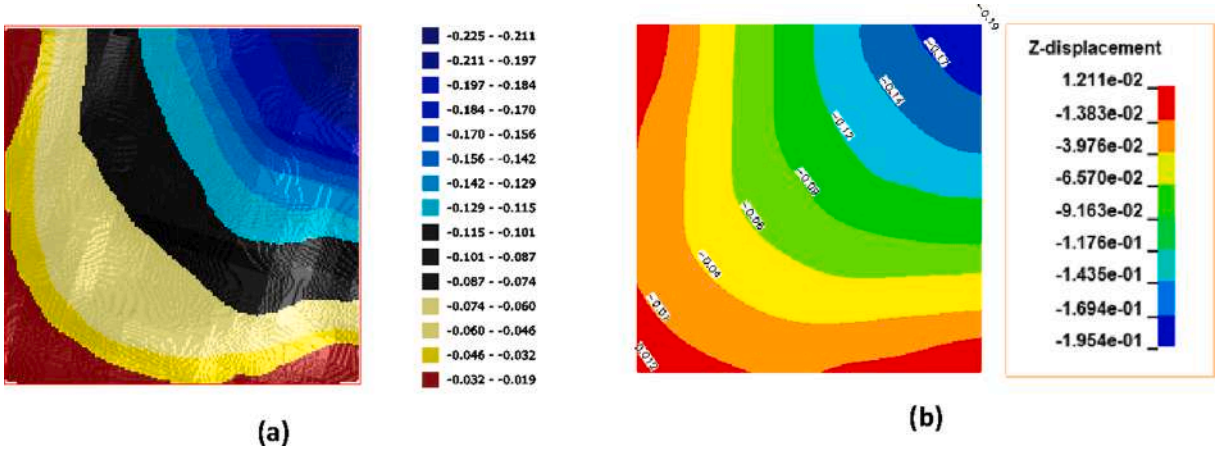

Fig. 18. Test (a) and FEM (b) Top Slab Deflection.

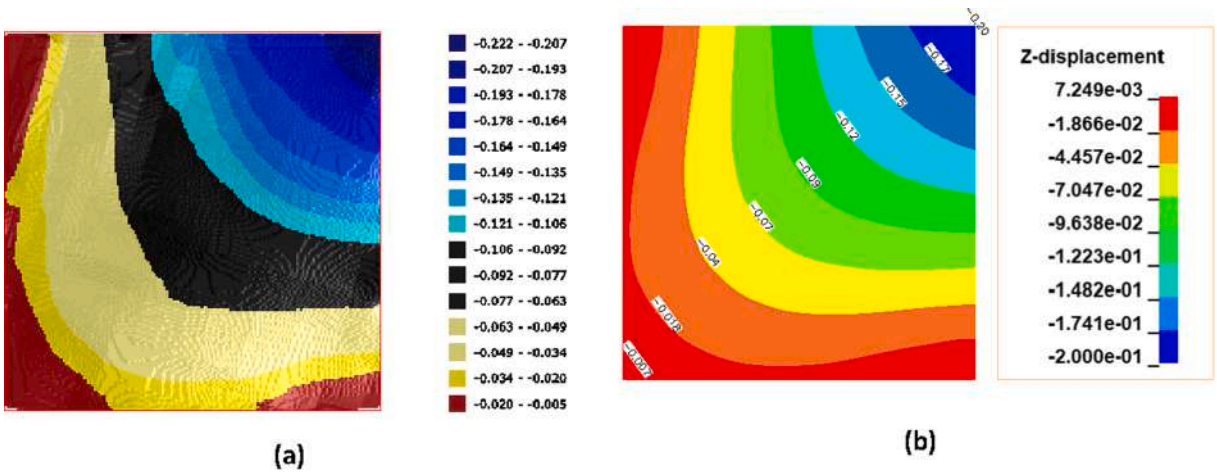

Fig. 19. Test (a) and FEM (b) Bottom Slab Deflection.

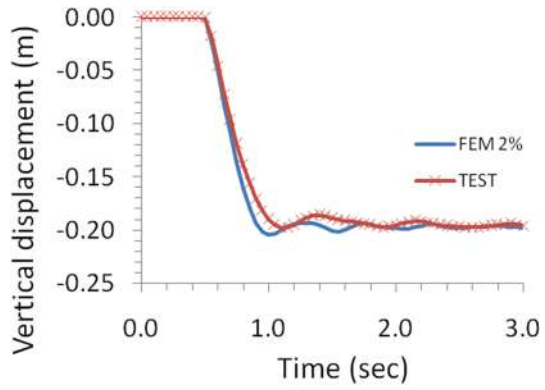

Fig. 20. Comparison of the displacement history from FEM model and test results.

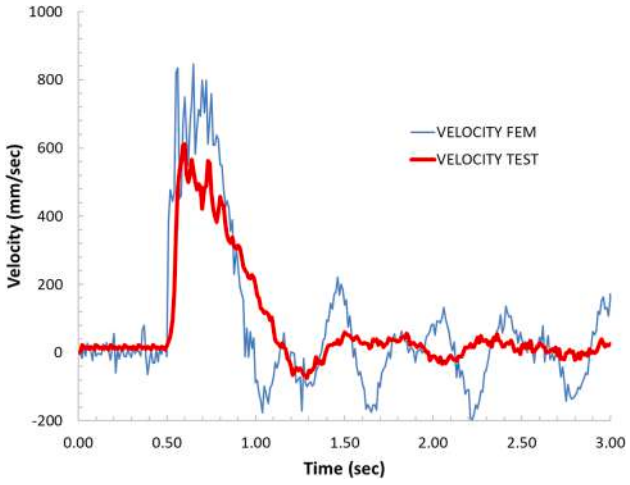

Fig. 21. Velocity of corner of slab. Comparison between experimental values and values obtained by FEM. The test value is obtained by numerical derivarion of the deflection results obtained by DIC.

5. Test results, general behaviour and comparison to model predictions

5.1. Material properties

The concrete was designed as class C25/30 according to [9]. The cement type used was Class S. Table 3 sumarizes all the compressive strength tests carried out on the concrete.

It was intended to test the slab at 28 days. However due to small construction delays, it was tested earlier, on May 4th 2016. At that time the bottom columns were 28 days old, the bottom slab 26, the columns supporting the top slab 23 and the top slab 20.

Table 4 shows the estimated concrete strength of each element on the day of the test. These values were estimated by using the equations for the evolution of concrete strength with time according to [9], assuming a value of $s = 0.38$ for a Class S cement, as shown in Fig. 9. In the figure the test results are also plotted using symbols.

5.2. Cracking patterns

This section presents a comparison between the observerd damage at the end of the test and the peak tensile strain concentrations from the LS-DYNA model. Although the LS-DYNA concrete material model does not explicity show the cracks that form on the surface, a reasonable approximation of crack location can be obtained by plotting the maximum principal strain at the solid integration points used to model the concrete material (eight node solid elements). Fig. 10 and Fig. 11 show the cracking patterns predicted by LS-DYNA on the top and bottom surfaces of the top and bottom slab, respectively. The crack pattern in the bottom face of the slabs is consistent with those of a slab working in sagging flexure along an axis with a span length corresponding to the diagonal line perpendicular to the symmetry axis. The diagonal cracks radiating from the supports on the top of the slab are compatible with those on a cantilever spanning parallel to the symmetry axis of the structure. This type of behaviour is also illustrated in [21] – see Fig. 12.

Fig. 13 and Fig. 14 show a comparison between the cracking pattern predicted by the FEM and the pattern observed in the test, it is evident that both patterns are very similar.

Fig. 15 shows the cracking pattern along the edge of the slabs. These are torsional cracks as their inclination is contrary to the inclination of shear cracks. The connection between the support and the first floor slab

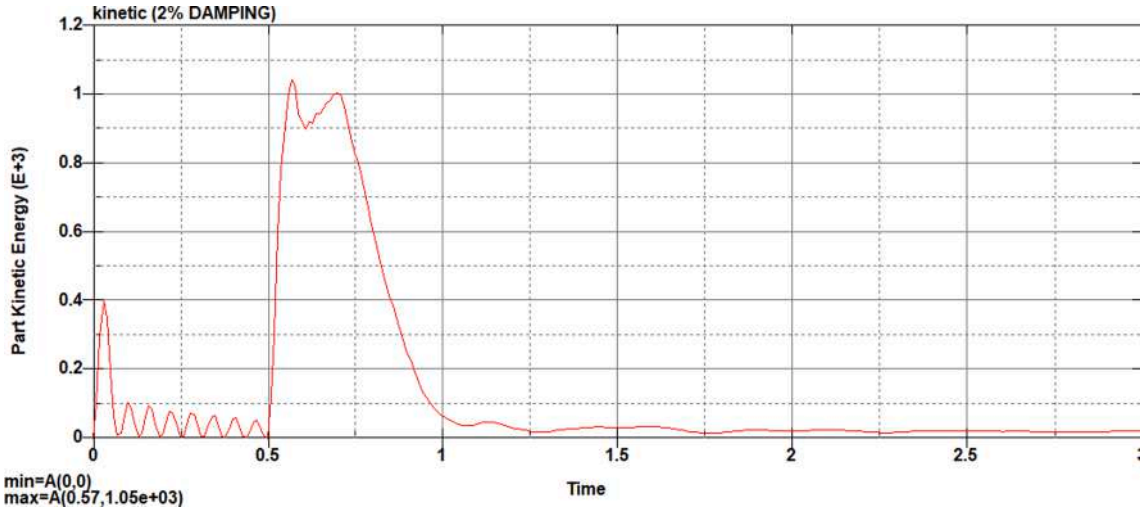

Fig. 22. Kinetic Energy of the structure determined by FEM analysis for 2% damping.

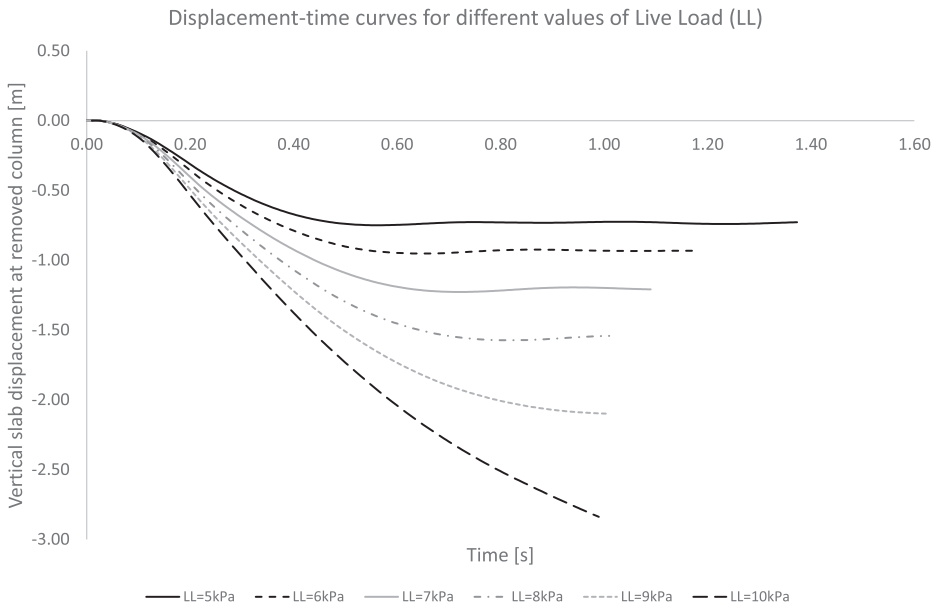

Fig. 23. Vertical slab displacement at location of removed column versus time for different values of live loads.

shows also such torsional cracks (see Fig. 16). This is a type of action for which the connection is not designed and failure of this connection could potentially lead to collapse of the structure. This type of cracking pattern, however does not develop at the connection between the column and the top slab because the rotation of the slab is accomodated by more extensive cracking (and possibly yielding of the reinforcement) at the top of the column (see Fig. 17). The horizontal cracks in the support at the top part of the top column were larger than those observed at the bottom suppports. This different behaviour is due to the difference in axial force as the compression force in the bottom column is roughly twice the compression in the top columns.

The stresses in the reinforcement are well within the serviceability limits and the width of the flexural cracks was small, around 0.2 mm.

5.3. Deflections

Fig. 18 and Fig. 19 show a comparison between the deflections measured by laser-scan and the prediction of the model. It can be seen that both the shapes and values obtained by the simulation are very close to those of the test. It is also worth noting that the value of the maximum deflection is relatively low and not sufficient to generate significant membrane action. This explains why the simple linear-elastic model with cracked stiffness presented in Section 4.1 also obtained a good approximation to the observed deflections.

Fig. 20 shows a comparison between the time history of displacements measured by DIC and the prediction of the FEM model using a reasonable damping index of 2%. This damping ratio has been selected due to the relatively small damage observed on the specimen. Cracks were small enough to be admissible in SLS. This damping index is within the range recommended by EN 1991-2 [8] for reinforced concrete railway bridges. It can be seen that there is good agreement between experimental and model results. A very interesting fact that can be derived from this figure is that the impact factor is quite low, as can be seen from the small magnitude of the oscillation of deflections after the collapse of the column. Reasons for this can be related to the asymmetry in stiffness as the slab is cracked when deflecting downwards, but not when deflecting upwards.

Immediately after the sudden column removal, static equilibrium is not satisfied and the deflections become larger in order to increase the strain energy of the system. This excess of external work is transformed

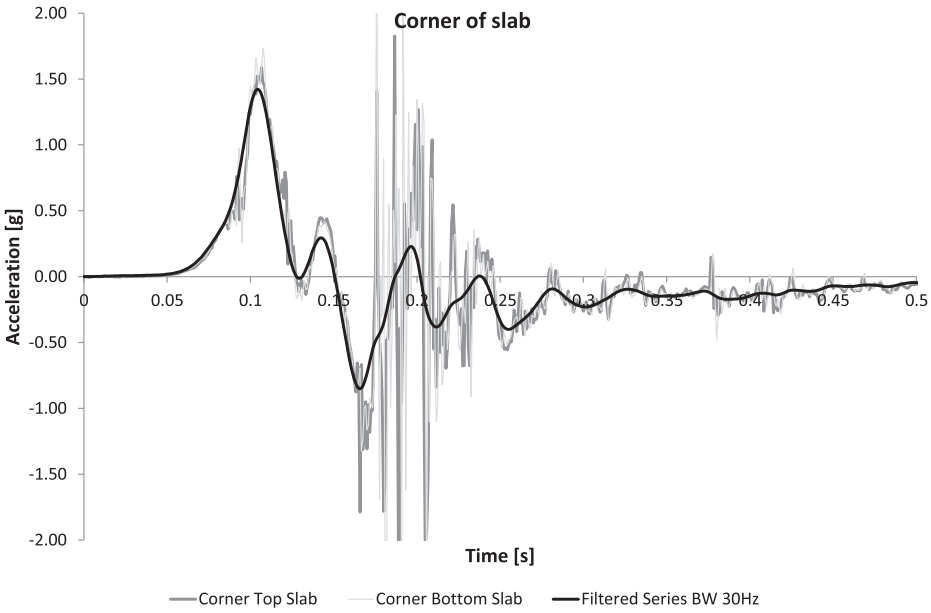

Fig. 24. Measured accelerations at the corner of the slab (over the removed column).

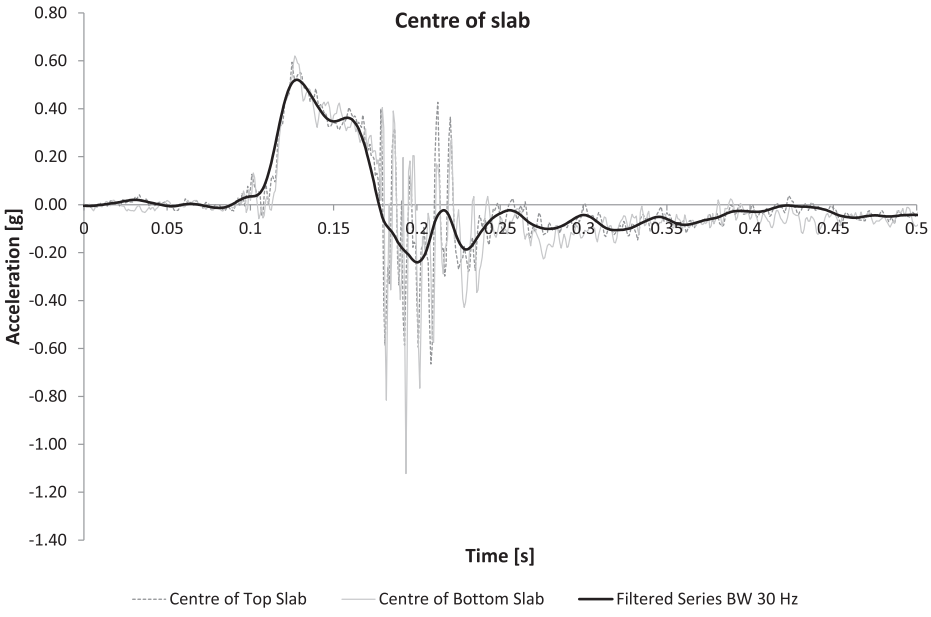

Fig. 25. Measured accelerations at the center of the slabs.

into kinetic energy, increasing the velocity of the structural system (see Fig. 21). As the structure deflects, the kinetic energy decreases, and the structure absorbs the potential energy of gravity loads in form of elastic and inelastic energy. The maximum dynamic response is reached when the work done by gravity loads is equal to the stored strain energy of the system, and hence the kinetic energy is zero (see Fig. 22).

Two hours after the test, deflections had not yet stabilized, even though their increase rate was very low. For safety reasons, it was decided to shore-up the structure. It is suspected that this behaviour could be related to continuing damage at the column-slab connection where inclined torsional cracks were seen to form. In another full-size experimental tests carried out in the framework of the same project as the two-storey structure reported here, a two span one storey reinforced concrete structure was also subjected to the demolition of one central column, an action it withstood well, and then to the demolition of the second central column. At this point the structure collapsed due to failure of the column-slab connection which showed a similar cracking pattern as that observed here. The results of this test are, as of yet, unpublished.

In order to be able to establish a basis of comparison with other tests, numerical analyses have been undertaken to try to assess the maximum load that could be carried by the structure. For this both slabs have been loaded with increasing values of live loads going from 5 kPa to 10 kPa. Fig. 23 shows the result. The structure seems to be stable up to a live load value of 9 kPa. For a larger value the slab would touch the floor as the deflection would exceed the height of the columns. The ratio between

the theoretical collapse load and the load applied during testing would be (6.25 + 9)/6.25 = 2.44 (where 6.25 = 0.25 × 25 kN/m^2 is the self weight of one slab).

6. Accelerations

Accelerations of the corner and the central point of both slabs were measured using high frequency accelerometers (1200 Hz). The measurements were taken applying a Butterworth filter for frequencies above 250 Hz. The signals were then reprocessed by applying a 2nd order Butterworth filter with a cut-off frequency of 30 Hz, since the significant structural vibrations modes were much below this figure. This second filter is able to remove a lot of noise that is present in the acceleration-time diagram as the slab reaches its maximum downwards deflection.

Fig. 24 and Fig. 25 show the measured accelerations at the corner and centre of the slab, respectively for both bottom and top slab. It can be seen that the measurements at both slabs are very coherent, so that both slabs have practically identical movements. This is also an indication of the correctness of the measurements. Notice that maximum accelerations when the slab is falling are greater than 1 g, which would be the maximum expected acceleration for the case of a free-falling body. The reason for this is that, with respect to its final equilibrium position, the slab is initially deformed in the upwards direction and has therefore stored strain energy. When the support fails, the slab is subjected to both gravity (which will accelerate the slab an amount *g)* and to the release of the stored strain energy, thereby explaining the initial acceleration peak of the corner .

7. Conclusions

From the above considerations, the following conclusions can be drawn:

1. The structural typology that was tested, a concrete frame with solid slabs has shown a robust behaviour when the edge column was suddenly removed (at the very least in the short/mean term – see 5. below). This result is significant given that the test was a full scale test on a specimen reinforced without accounting for column loss.
2. The deflection of the structure was only 22 cm, corresponding to a deflection to diagonal span ratio of only 2.2%, so that no significant membrane forces developed.
3. The cracking pattern and the crack widths show that, after column collapse, the slab resisted the forces mainly by sagging flexure along the axis of symmetry, with some contribution of the top reinforcement, especially near the columns.
4. The measured impact factor was very low, as the amplitude of oscillations around the equilibrium position were seen to be quite small.
5. Even though the apparent damage was low, after two hours the deflections had not yet fully stabilized and the structure was shored. It is suspected that this behaviour may be related to the deterioration of the column-slab connection, whose failure could eventually lead to the collapse of the complete structure due to its potential brittleness. Nonetheless, numerical analysis predicts that the struture would be able to withstand, with much larger deflections, a total load of up to 2.44 times the applied dead load.
6. The behaviour of the structure could be closely modelled using FEM both in the qualitative behaviour (cracking patterns) and the quantitative behaviour (deflections). The excellent match between theoretical and experimental results is probably related to the limited plasticity behaviour developed by the structure. Such good results can of course be reached with FEM for more complex problems, but, in such cases some calibration of the model parameters is usually needed.

Declaration of Competing Interest

The authors declare that they have no known competing financial interests or personal relationships that could have appeared to influence the work reported in this paper.

Acknowledgements

The test described in this paper was carried out within the framework of research project IPT-2012-0845-370000 (ITSAFE), involving DRAGADOS, FHECOR and the Universidad Politécnica de Madrid (UPM). This research project had the financial support of the Spanish Ministry of Economy and Competitivity under the INNPACTO program.

The authors are grateful to Francisco Gálvez and Victor Rey for their help with the DIC measurements and to Carlos Zanuy for his help with the measurement of accelerations.

Appendix A. Supplementary material

Supplementary data to this article can be found online at https://doi.org/10.1016/j.engstruct.2021.112411.

References

[1] Alshaikh IM, Abu Bakar B, Alwesabi EA, Akil HM. Experimental investigation of the progressive collapse of reinforced concrete structures: An overview. Structures 2020;25:881–900.
[2] ASCE/SEI. ASCE/SEI 7-16: Minimum Design Loads and Associated Criteria for Buildings and Other Structures. Reston, VA, USA: ASCE; 2016.
[3] Baker A. Partial stability - Tests on concrete beams and slabs. Leningrad: CEB Comission VI; 1972.
[4] Bao Y, Kunnath S, El-Tawil S, Lew H. Macromodel-based simulation of progressive collapse: RC frame structures. J Struct Eng (ASCE) 2008;134(7):1079–91.
[5] Brunesi E, Nacimbene R. Extreme response of reinforced concrete buildings through fiber force-based finite element analysis. Eng Struct 2014;69:206–15.
[6] Brunesi E, Parisi F. Progressive collapse fragility models of RC framed buildings based on pushdown analysis based on pushdown analysis. Eng Struct 2017;152:579–96.
[7] Brunesi E, Nascimbene R, Parisi F, Augenti N. Progressive collapse fragility of reinforced concrete framed structures through incremental dynamic analysis. Eng Struct 2015;104:65–79.
[8] CEN. EN 1991–2: Actions on structures - Part 2: Traffic loads on bridges. Brussels: Comité Européen de Normalisation; 2003.
[9] CEN. EN 1992-1-1: Design of concrete structures - Part 1–1: General rules and rules for buildings. Brussels: Comité Européen de Normalisation; 2004.
[10] CEN. EN 1991-1-7 Eurocode 1 - Actions on structures - Part 1–7: General Actions - Accidental Actions. Brussels: Comité Européen de Normalisation; 2006.
[11] DoD. UFC 4-023-03 Design of Buildings to Resist Progressive Collapse. Washington, D.C.: Department of Defense; 2009.
[12] Eren N, Brunesi E, Nascimbene R. Influence of masonry infills on the progressive collapse resistance of reinforced concrete framed buildings. Eng Struct 2019;178:375–94.
[13] Fomento Md. EHE - Instrucción de Hormigón Estructural. Madrid: Ministerio de Fomento - Secretaría General Técnica; 1999.
[14] GSA. Alternate Path Analysis & Design Guidelines for Progressive Collapse resistance. Washington D.C.: General Services Administration; 2013.
[15] Hallquist J. LS-Dyna Theory Manual. Livermore, California, USA: Livermore Software Technology Corporation; 2006. Obtenido de http://www.lstc.com/pdf/ls-dyna_theory_manual_2006.pdf.
[16] Jose M. Adam, M. B. (2020). Dynamic performance of a real-scale reinforced concrete building test under a corner-column failure scenario. Engineering Structures, 210. doi:https://doi.org/10.1016/j.engstruct.2020.110414.
[17] Krauthammer T. Blast-resistant structural concrete and steel connections. Int J Impact Eng 1999:887–910.
[18] Kunnath SK, Bao Y, El-Tawil S. Advances in computational simulation of gravity-induced disproportionate collapse of RC frame buildings. J Struct Eng 2018;144(2):03117003.
[19] Lee C-H, Kim S, Han K-H, Lee K. Simplified nonlinear progressive collapse analysis of welded steel moment frames. J Constr Steel Res 2009;65:1130–7.
[20] Marjanishvili S. Progressive analysis procedure for progressive collapse. J Perform Constr Facil 2004:79–85.
[21] Melo GS. Behaviour of reinforced concrete flat slabs after local failure. London: The Polytechnic of Central London; 1990.
[22] Murray YD. Theory and evaluation of concrete material model 159. 8th International LS-DYNA users conference, (págs. 25-35). Michigan, USA; 2004.
[23] Nakao M. Chain Reaction Collapse of Hight-rise Apartment due to a Gas Explosion – May 16, 1968 in Ronan Point, East London, England. Failure Knowledge Database / 100 Selected Cases. JST; 2005.

[24] NIST. NISTIR 7396 - Best Practices for Reducing the Potential for Progressive Collapse in Buildings. Washington, D.C.: Department of Commerce; 2007.
[25] Parisi F, Scalvenzi M, Brusesi E. Performance limit states for progressive collapse analysis of reinforced concrete framed buildings. Struct Concr 2019;20(1):68–84.
[26] Pérez Caldentey A, Padilla Lavaselli P, Corres Peiretti H, Ariñez Fernández F. Influence of stirrup detailing on punching shear strength of flat slabs. Eng Struct 2013;49:855–65.
[27] Pham AT. Numerical investigations on static and dynamic responses of reinforced concrete sub-assemblages under progressive collapse. Eng Struct. 2017;149:2–20.
[28] Qian Ka. Experimental study of drop-panel effects on response of reinforced concrete flat slabs after loss of corner column. ACI Struct J 2013;110(2):319–29.
[29] Regan P. Partial stability at damaged corners of framed buildings - Tests of a flat slab structure. London: Polytechinic of Central London; 1973.
[30] Regan P. Catenary test of cmposite (precast/in situ) concrete floors. Report to the Department of Environment. London: Polytechnic of Central London; 1974.
[31] Regan P. ACI SP. 48 Catenary action in damaged concrete structures. En A. C. Institute, Special Publication 48 (págs. 1991-224). Farmington Hill, MI: ACI; 1975.
[32] Sasani M. Response of a reinforced concrete infilled-frame structure to removal of two adjacent columns. Eng Struct 2008;30:2478–91.
[33] Song BA, Giriunas KA, Sezen H. Progressive collapse testing and analysis of a steel frame building. J Constr Steel Res 2014;94:76–83.
[34] Wang J, Wang W, Bao Y. Full-scale test of a steel-concrete composite floor system with moment-resisting connections under a middle-edge column removal scenario. J Struct Eng 2020;146(5):04020067.
[35] Xiao YK. Collapse test of a 3-story 3-span half-scale. ACI Struct J 2015;112(4):429–38.
[36] Yu JT. Experimental and numerical investigation on progressive collapse resistance of reinforced concrete beam column sub-assemblies. Eng Struct 2013:90–106.
[37] Zandonini R, Baldassino N, Freddi F, Roverso G. Steel-concrete frames under the column loss scenario: An experimental study. J Constr Steel Res 2019;162:105527.
[38] Zhang Q, Li Y. Experimental and modeling study on the progressive collapse resistance of a reinforced concrete frame structure under a middle column removal scenario. The Struct Des Tall Special Build 2020;29.